Cell Research (2017) 27:1216-1230.

www.nature.com/cr

ORIGINAL ARTICLE

Mettl3-/Mettl14-mediated mRNA N^6-methyladenosine modulates murine spermatogenesis

Zhen Lin[1], Phillip J Hsu[2, *], Xudong Xing[3, *], Jianhuo Fang[3], Zhike Lu[2], Qin Zou[3], Ke-Jia Zhang[1], Xiao Zhang[4], Yuchuan Zhou[1], Teng Zhang[1], Youcheng Zhang[1], Wanlu Song[3], Guifang Jia[4], Xuerui Yang[3], Chuan He[2, 4], Ming-Han Tong[1]

[1]State Key Laboratory of Molecular Biology, Shanghai Key Laboratory of Molecular Andrology, CAS Center for Excellence in Molecular Cell Science, Shanghai Institute of Biochemistry and Cell Biology, Chinese Academy of Sciences, University of Chinese Academy of Sciences, Shanghai 200031, China; [2]Department of Chemistry, Department of Biochemistry and Molecular Biology, Institute for Biophysical Dynamics, Howard Hughes Medical Institute, The University of Chicago, 929 East 57th Street, Chicago, IL 60637, USA; [3]MOE Key Laboratory of Bioinformatics, Center for Synthetic & Systems Biology, THU-PKU Center for Life Sciences, School of Life Sciences, Tsinghua University, Beijing 100084, China; [4]Synthetic and Functional Biomolecules Center, Beijing National Laboratory for Molecular Sciences, Key Laboratory of Bioorganic Chemistry and Molecular Engineering of Ministry of Education, College of Chemistry and Molecular Engineering, Peking University, Beijing 100871, China

Spermatogenesis is a differentiation process during which diploid spermatogonial stem cells (SSCs) produce haploid spermatozoa. This highly specialized process is precisely controlled at the transcriptional, posttranscriptional, and translational levels. Here we report that N^6-methyladenosine (m^6A), an epitranscriptomic mark regulating gene expression, plays essential roles during spermatogenesis. We present comprehensive m^6A mRNA methylomes of mouse spermatogenic cells from five developmental stages: undifferentiated spermatogonia, type A_1 spermatogonia, preleptotene spermatocytes, pachytene/diplotene spermatocytes, and round spermatids. Germ cell-specific inactivation of the m^6A RNA methyltransferase *Mettl3* or *Mettl14* with *Vasa-Cre* causes loss of m^6A and depletion of SSCs. m^6A depletion dysregulates translation of transcripts that are required for SSC proliferation/differentiation. Combined deletion of *Mettl3* and *Mettl14* in advanced germ cells with *Stra8-GFPCre* disrupts spermiogenesis, whereas mice with single deletion of either *Mettl3* or *Mettl14* in advanced germ cells show normal spermatogenesis. The spermatids from double-mutant mice exhibit impaired translation of haploid-specific genes that are essential for spermiogenesis. This study highlights crucial roles of mRNA m^6A modification in germline development, potentially ensuring coordinated translation at different stages of spermatogenesis.

Keywords: m^6A RNA modification; Mettl3; Mettl14; spermatogonial stem cell; spermiogenesis
Cell Research (2017) **27**:1216-1230. doi:10.1038/cr.2017.117; published online 15 September 2017

Introduction

Spermatogenesis is a complex developmental process that typically consists of three stages: mitosis, meiosis, and spermiogenesis [1, 2]. In mammals, SSCs either self-renew or undergo repeated mitotic divisions to generate A paired (A_{pr}) and A aligned (A_{al}) spermatogonia [3]. The A_{al} spermatogonia differentiate into A_1 spermatogonia and subsequently form type B spermatogonia through a series of mitotic divisions. The type B spermatogonia give rise to primary spermatocytes that enter the meiotic phase, in which reduced division and genetic recombination occur, resulting in the formation of haploid round spermatids. Next, during spermiogenesis, round spermatids undergo extensive morphological and biochemical transformations to differentiate into elongated mature spermatozoa. These processes are precisely controlled

*These two authors contributed equally to this work.
Correspondence: Ming-Han Tong[a], Chuan He[b], Xuerui Yang[c]
[a]Tel: 86-21-5492-1264
E-mail: minghan@sibcb.ac.cn
[b]E-mail: chuanhe@uchicago.edu
[c]E-mail: yangxuerui@tsinghua.edu.cn
Received 27 July 2017, revised 8 August 2017, accepted 15 August 2017; published online 15 September 2017

by complex regulatory programs at the transcriptional, posttranscriptional, and translational levels. These programs direct the proper expression of specific sets of genes at different developmental stages [4]. For example, transcription ceases in elongated spermatids due to chromatin compaction. All mRNAs required for the late stage of spermiogenesis are transcribed in spermatocytes and round spermatids and stored steadily until they are needed [4]. Posttranscriptional and translational controls of stored mRNAs, therefore, ensure timely synthesis of proteins essential for the transcriptionally silent spermatids [4]. Although posttranscriptional and translational regulation are important for the appropriate expression of specific genes in spermatogenesis, limited knowledge exists about how this regulation is achieved in male germ cells. Thus, mammalian spermatogenesis provides a powerful system for studying gene regulation at the posttranscriptional and translational levels.

Emerging evidence has shown that N^6-methyladenosine (m^6A), the most prevalent mammalian internal mRNA modification, is implicated in regulation of nearly every aspect of the mRNA life cycle, including pre-mRNA splicing, mRNA export, stability, and translation [5-10], and is thus crucial for various cellular, developmental, and disease processes such as heat shock response [11], DNA repair [12], circadian rhythm [13], maternal to zygotic transition [14], and tumorigenesis [15-17]. In mammals, the m^6A modification is catalyzed by a multicomponent methyltransferase complex that includes methyltransferase-like 3 (METTL3) [18], METTL14 [19], and Wilms' tumor 1-associated protein (WTAP) [20], and can be demethylated into adenosine by two known demethylases: fat mass and obesity-associated factor (FTO) [21], and AlkB homologue 5 (ALKBH5) [22]. Several studies have shown that depletion of *Mettl3* and *Mettl14* (or their homologs in other species) caused a block in embryonic stem cell self-renewal and differentiation [23, 24], embryonic developmental defects, sex reversal [25, 26], and impaired gametogenesis [22, 27, 28] in diverse organisms. Because m^6A is a newly discovered mechanism to coordinate translation and turnover of eukaryotic transcripts, we decided to study whether m^6A on mRNA may play critical roles to ensure proper regulation of genes in mammalian spermatogenesis at the posttranscriptional and translational levels.

Here we show that m^6A is dynamically regulated and plays crucial roles to shape gene expression in SSC development and during spermatogenesis. We reveal that lack of m^6A by germ cell-specific inactivation of *Mettl3* or *Mettl14* results in SSC depletion due to significant changes in translational efficiency (TE). Double deletion of *Mettl3* and *Mettl14* in advanced germ cells leads to impaired spermiogenesis due to altered TE of m^6A-containing transcripts. This study thus reveals m^6A-dependent translation as a previously undefined mechanism that modulates protein synthesis in SSCs and in spermatids, highlighting a crucial role of m^6A on mRNA in translational regulation, particularly of transcription-ceasing cells and in mammalian development.

Results

Germ cell-specific knockout of Mettl3 or Mettl14 causes loss of m^6A, resulting in depletion of SSCs

To explore the roles of m^6A in spermatogenesis, we first examined whether two m^6A writers, METTL3 and METTL14, are expressed in mouse testes, and found that both proteins localize to the nucleus of male germ cells (Supplementary information, Figure S1A and S1B). We then generated a *Mettl3*-floxed line and a *Mettl14*-floxed line using a CRISPR/Cas9 system (Supplementary information, Figure S1C). *Mettl3*$^{f/\Delta}$*Vasa-Cre* (hereafter referred to as *Mettl3*-vKO) mice were obtained to specifically inactivate *Mettl3* in male germ cells as early as embryonic day 15 (E15) [29] (Supplementary information, Figure S1C). Immunostaining confirmed the absence of METTL3 protein in the male germ cells (Supplementary information, Figure S2). Analysis of m^6A levels with quantitative ultra-performance liquid chromatography coupled with tandem mass spectrometry (UPLC-MS/MS) in purified mRNA from control and *Mettl3*-vKO THY1$^+$ undifferentiated spermatogonia showed that *Mettl3* deficiency significantly but incompletely decreased m^6A levels by ~ 70% (Figure 1A). *Mettl3*-vKO males are sterile. Histological analyses of the *Mettl3*-vKO testes showed clear defects in the development of SSCs (Figure 1B-1H, Supplementary information, Figure S3A-S3G). However, *Mettl3*-vKO testes contained normal numbers of gonocytes at birth. By 6 weeks after birth, histological staining and immunostaining showed that seminiferous epithelium in *Mettl3*-vKO testes were completely devoid of any germ cells, with only SOX9-positive Sertoli cells remaining (Figure 1C-1F). The number of undifferentiated spermatogonia (PLZF-positive cells) in *Mettl3*-vKO testes was similar to that in the controls up to P5 but significantly reduced by P7 (Supplementary information, Figure S3A-S3C). Moreover, there was little if any difference in apoptosis of PLZF-positive spermatogonia between control and *Mettl3*-vKO testes (Supplementary information, Figure S3D and S3E). Furthermore, we found that EdU incorporation was significantly increased in GFRα1-positive A_{single} (A_s) spermatogonia, the most primitive set of spermatogonia, from *Mettl3*-vKO testes compared to those from controls, indicating higher pro-

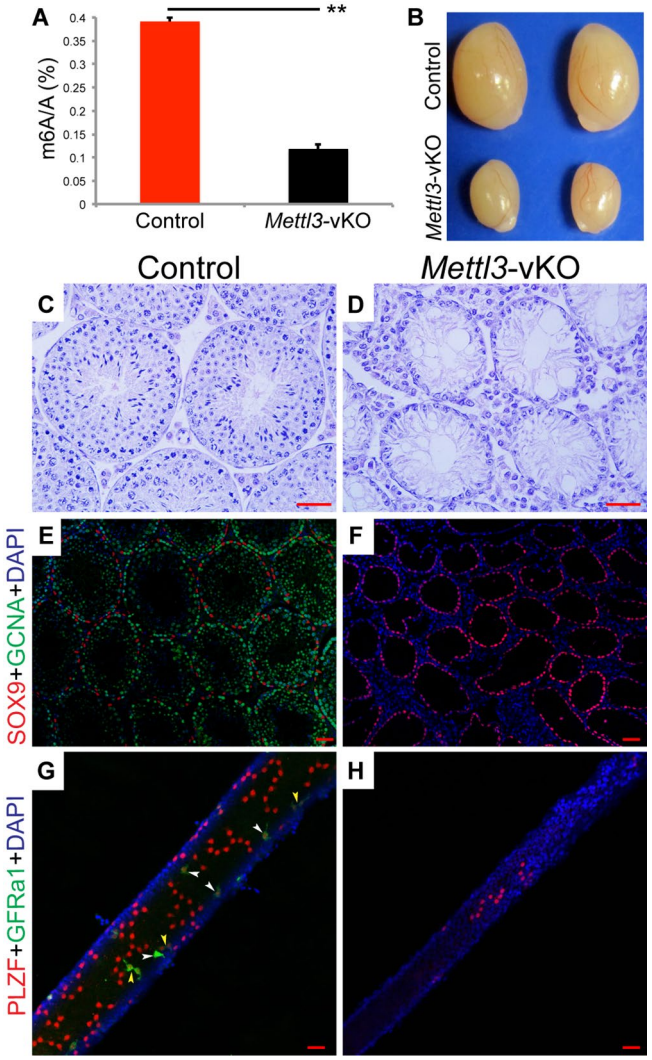

Figure 1 Characterization of germ cell-specific *Mettl3* mutants. **(A)** UPLC-MS/MS analysis of m^{6}A percentage relative to adenosine in purified mRNA from the undifferentiated spermatogonia of controls and *Mettl3*-vKO mutants. Data are expressed as mean ± SD from two biological replicates. $^{**}P < 0.01$, Student's *t*-test. **(B)** Gross morphology of representative testes from an adult control and age-matched *Mettl3*-vKO mutant. **(C**, **D)** H&E staining of control **(C)** and *Mettl3*-vKO **(D)** testes at age of 6 weeks. **(E**, **F)** Immunohistochemical staining for germ-cell marker GCNA (green), Sertoli cell marker SOX9 (red), and DAPI (blue) in sections of 6-week-old control **(E)** and *Mettl3*-vKO mutant **(F)** testes. **(G**, **H)** Whole-mount immunostaining of seminiferous tubules for GFRα1 (a marker for early stage of the undifferentiated spermatogonia, Green), PLZF (a marker for the undifferentiated spermatogonia, red), and DAPI (blue) in 4-week-old controls **(G)** and *Mettl3*-vKO mutants **(H)**. White and yellow arrowheads indicate both GFRα1- and PLZF-positive representative A_s and A_p spermatogonia, respectively, in controls, whereas there are no A_s and even A_p spermatogonia in mutants. (Scale bar, 40 μm).

liferation of SSCs after *Mettl3* depletion (Supplementary information, Figure S3F and S3G). Consistent with this, A_s spermatogonia were lost in the *Mettl3*-vKO testes at the age of 4 weeks; however, $A_{aligned}$ (A_{al}) spermatogonia, which are derived from A_s spermatogonia, remained, demonstrating that the exhaustion of SSC pool is possibly due to SSC excessive proliferation after *Mettl3* deletion (Figure 1G and 1H). Consistent with the notion that m^{6}A is a key marker to determine cell state as previously shown [14, 23, 30], loss of m^{6}A upon *Mettl3* deficiency results in the loss of SSCs, causing depletion of germ cells in the *Mettl3*-vKO mice.

We also found that *Mettl14*$^{f/\Delta}$*Vasa-Cre* (hereafter referred to as *Mettl14*-vKO) males showed an equivalent decrease in m^{6}A levels on mRNA from germ cells and exhibited very similar SSC defects as compared to the *Mettl3*-vKO mice (Figure 2A-2H), suggesting that ablation of a single methyltransferase is sufficient to elicit SSC phenotypes. To test whether *Mettl3* and *Mettl14* could compensate for each other in SSCs, we generated double-mutant mice. We found the homozygous mutants (*Mettl3*$^{f/\Delta}$/*Mettl14*$^{f/\Delta}$*Vasa*-Cre, hereafter referred to as *Mettls*-vKO) displayed similar phenotypes to the *Mettl3* or *Mettl14* single-mutants (Supplementary information, Figure S4), suggesting there is no obvious compensative effect between *Mettl3* and *Mettl14*. Collectively, these findings reveal that *Mettl3* and *Mettl14* control similar physiological processes in SSCs, consistent with the discovery that formation of a methyltransferase complex is required for m^{6}A deposition [31].

Combination deletion of Mettl3 and Mettl14 leads to impaired spermiogenesis

We next asked whether m^{6}A plays a role in meiosis and/or spermiogenesis. To test this, we first conditionally deleted either *Mettl3* or *Mettl14* in advanced germ cells with *Stra8-GFPCre*, respectively. *Stra8-GFPCre* induces recombination starting from type A_1 spermatogonia (before meiosis). We found that *Mettl3*$^{f/\Delta}$*Stra8-GFPCre* (hereafter referred to as *Mettl3*-sKO), and *Mettl14*$^{f/\Delta}$ *Stra8-GFPCre* (hereafter referred to as *Mettl14*-sKO) male mice are fertile. Histological and immunohistochemical analysis showed normal spermatogenesis occurring in both *Mettl3*-sKO and *Mettl14*-sKO mice (Supplementary information, Figure S5A-S5O). Immunostaining verified that either METTL3 or METTL14 protein was absent in the respective mutant advanced germ cells, revealing high KO efficiency in both lines (Supplementary information, Figure S6A and S6B). By UPLC-MS/MS, we observed a 55-65% decrease in m^{6}A levels in *Mettl3*-sKO or *Mettl14*-sKO pachytene spermatocytes, and a 45% decrease in round spermatids

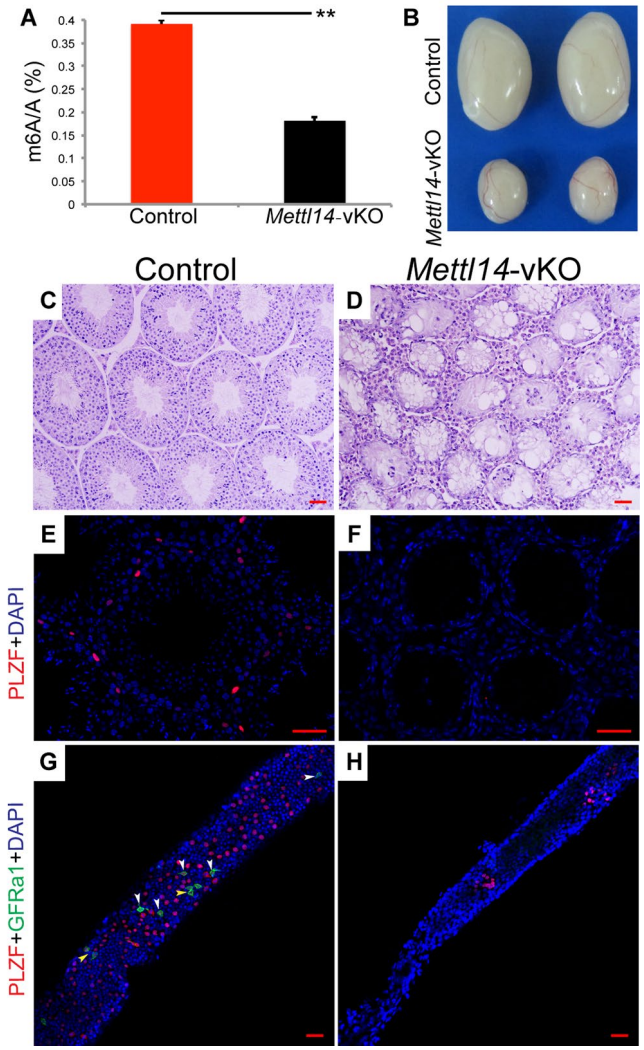

Figure 2 Characterization of germ cell-specific *Mettl14* mutants. **(A)** UPLC-MS/MS analysis of m^{6}A percentage relative to adenosine in purified mRNA from the undifferentiated spermatogonia of controls and *Mettl14*-vKO mutants. Data are expressed as mean ± SD from two biological replicates. $^{**}P < 0.01$, Student's *t*-test. **(B)** Gross morphology of representative testes from an adult control and age-matched *Mettl14*-vKO mutant. **(C**, **D)** H&E staining of control **(C)** and *Mettl14*-vKO **(D)** testes at age of 6 weeks. **(E**, **F)** Immunohistochemical staining for the undifferentiated spermatogonia marker PLZF (red) and DAPI (blue) in sections of 6-week-old control **(E)** and *Mettl14*-vKO mutant **(F)** testes. **(G**, **H)** Whole-mount immunostaining of seminiferous tubules for GFRα1 (green), PLZF (red), and DAPI (blue) in 4-week-old controls **(G)** and *Mettl14*-vKO mutants **(H)**. White and yellow arrowheads indicate both GFRα1- and PLZF-positive representative A_s and A_p spermatogonia, respectively, in controls **(G)**. There is no A_s, even A_p spermatogonia in *Mettl14*-vKO mutants **(H)**. (Scale bar, 40 μm.)

relative to controls (Figure 3A and Supplementary information, Figure S7D).

We then conditionally inactivated both *Mettl3* and *Mettl14* in advanced germ cells with *Stra8-GFPCre*. Testes from adult *Mettl3*$^{f/\Delta}$/*Mettl14*$^{f/\Delta}$*Stra8-GFPCre* (hereafter referred to as *Mettls*-sKO) double-mutants were significantly smaller than control littermate testes (Supplementary information, Figure S7A and S7B). Immunostaining demonstrated the absence of METTL3 and METTL14 proteins in the advanced germ cells of *Mettls*-sKO testes (Supplementary information, Figure S7C). The m^{6}A levels in spermatids of *Mettls*-sKO double mutants were significantly reduced compared to those in *Mettl3* and *Mettl14* single-mutant mice (Figure 3A). Interestingly, the differences in m^{6}A levels between *Mettls*-sKO double-mutant and single-mutant spermatocytes were not significant (Supplementary information, Figure S7D). Histological analysis showed that seminiferous tubules contained very few mature spermatozoa in mutants (Figure 3B). Consistent with this, decreased sperm levels were found in *Mettls*-sKO epididymis compared to those in controls (Figure 3B). Sperm counting further showed that the number of caudal epididymal sperm in the *Mettls*-sKO mice was only about 2% of that in control mice (Figure 3C). Computer-assisted sperm analysis (CASA) revealed that sperm motility was severely destroyed in the *Mettls*-sKO mice as compared to controls, indicating defects in sperm flagella (Figure 3C). More than 80% of the caudal epididymal sperm from *Mettls*-sKO mice displayed abnormal heads (Figure 3D; Supplementary information, Figure S7E and S7F). Altogether, these abnormalities resemble those found in human oligo-astheno-teratozoospermia (OAT) syndrome. Given that yeast *METTL3* orthologue *ime4* is shown to be critical for meiosis [28, 32-34], we expected a meiotic defect in *Mettls*-sKO mice. Unexpectedly, close examination of *Mettls*-sKO seminiferous tubules revealed no detectable abnormalities in germ cells of subsequent stages up to step 12 of elongating spermatids (Supplementary information, Figure S8), suggesting that the *Mettls*-sKO mice are normal in meiosis during spermatogenesis. The number of elongated spermatids (step 13 afterwards) dramatically decreased in the *Mettls*-sKO mice, and the heads of the *Mettls*-sKO mutant sperm were abnormal (Supplementary information, Figure S8). Thus, mRNA m^{6}A modification produced by *Mettl3* and *Mettl14* is essential for spermatid differentiation in late stages of spermiogenesis. Given that mice with a conditional mutation for either *Mettl3* or *Mettl14* show normal meiosis and spermiogenesis, these results indicate that these two enzymes could have different or partially overlapping functions in late spermatogenesis. This observation also suggests the presence of additional factors that may mediate mRNA

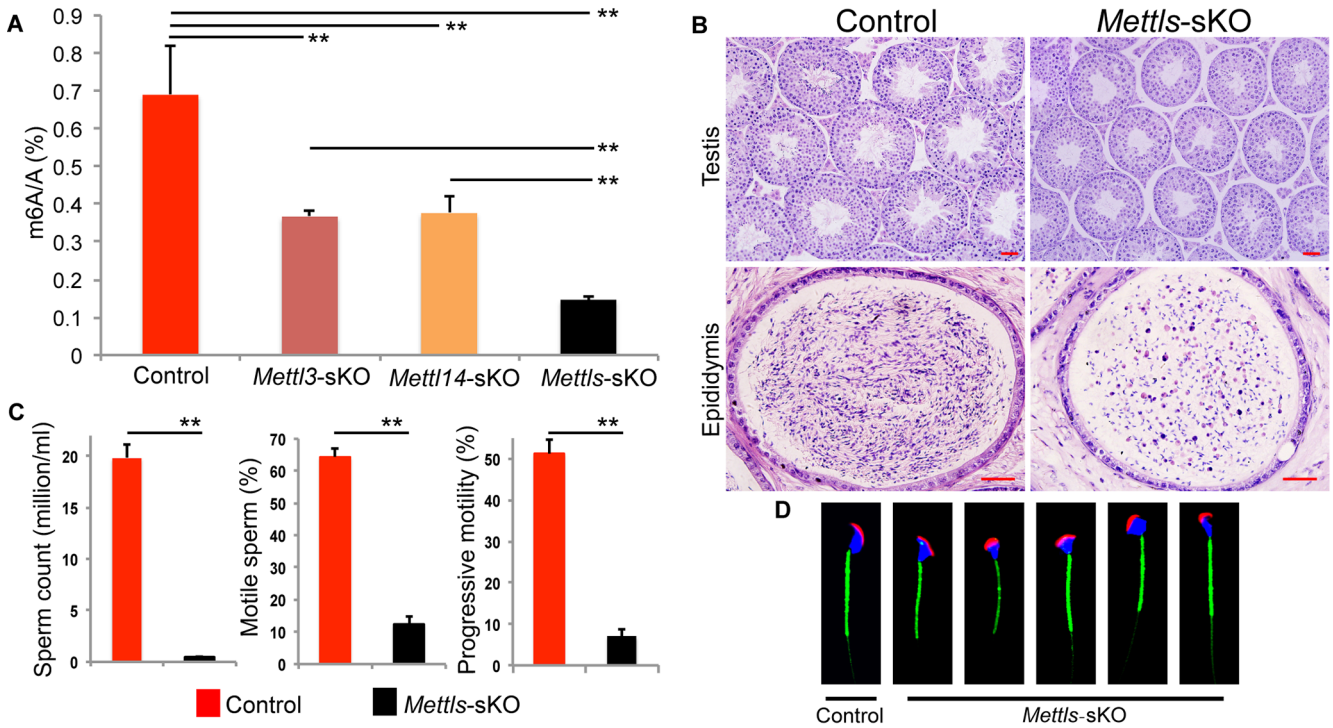

Figure 3 Analysis of advanced germ cell-specific *Mettl3* and *Mettl14* double-mutants. **(A)** m^{6}A LC-MS/MS quantification in spermatid of control and different knockout mice. The data show the mean ± SD of two biological replicates, $^{**}P < 0.01$, Student's *t*-test. **(B)** Morphology of testes and epididymis, from controls and *Mettls*-sKO double mutants. (Scale bars: 40 μm). **(C)** Number, total, and progressive motility of caudal epididymal sperm from 2-month-old control and *Mettls*-sKO double-mutant mice. Error bars represent SD, $^{**}P < 0.01$, Student's *t*-test (n = 5-6). **(D)** Fluorescence staining of caudal epididymal sperms from controls and *Mettls*-sKO mutants with fluorescence dye-labeled peanut lectin (PNA, red) for acrosome, MitoTracker Green FM (green) for mitochondria, and DAPI (blue), respectively.

methylation, as suggested in a recent study [35]. It will be of interest to test this hypothesis in the future.

Dynamic regulation of m^{6}A in SSC development and during spermatogenesis

To elucidate the role of m^{6}A in different stages of spermatogenesis, we first performed quantitative UPLC-MS/MS to monitor m^{6}A levels on mRNA from six developmental stages of mouse spermatogenic cells: Thy1$^+$ undifferentiated spermatogonia (including SSCs/progenitor cells), type A$_1$ spermatogonia, preleptotene spermatocytes, leptotene/zygotene spermatocytes, pachytene/diplotene spermatocytes, and round spermatids. We found that m^{6}A was present in all mRNA samples tested, with particularly high enrichment in pachytene/diplotene spermatocytes and round spermatids (Figure 4A). To further characterize the dynamic nature of m^{6}A in male germ cells during spermatogenesis, we performed m^{6}A affinity purification and sequencing (m^{6}A-seq) on purified mRNA from five developmental stages of mouse spermatogenic cells: Thy1$^+$ undifferentiated spermatogonia (including SSCs/progenitor cells), type A$_1$ spermatogonia, preleptotene spermatocytes, pachytene/diplotene spermatocytes, and round spermatids [6]. From the above five samples, we identified 23 031, 16 392, 18 479, 15 656, and 10 950 m^{6}A peak sites within the transcripts of 12 659, 12 167, 11 363, 11 293, and 12 491 genes, respectively, of which 9 092, 7 320, 7 471, 6 717, and 5 617 contained m^{6}A (Supplementary information, Figure S9A and Table S1). Consistent with previous findings [6, 7], we found that m^{6}A was present predominantly on its consensus motif of DRACH (D = A,G,U; R = A,G; H = A,C,U) at all five stages (Supplementary information, Figure S9B). m^{6}A was distributed throughout mRNA transcripts, with increased read density in the CDS and stop codon (Figure 4B). The overall distribution of m^{6}A peaks shifted dynamically between the five cell types. Notably, m^{6}A read density in the CDS of pachytene/diplotene spermatocytes and round spermatids was greater than that of undifferentiated spermatogonia, A1 spermatogonia, and preleptotene spermatogonia, reflecting the UPLC-MS/MS findings (Figure 4A and 4B).

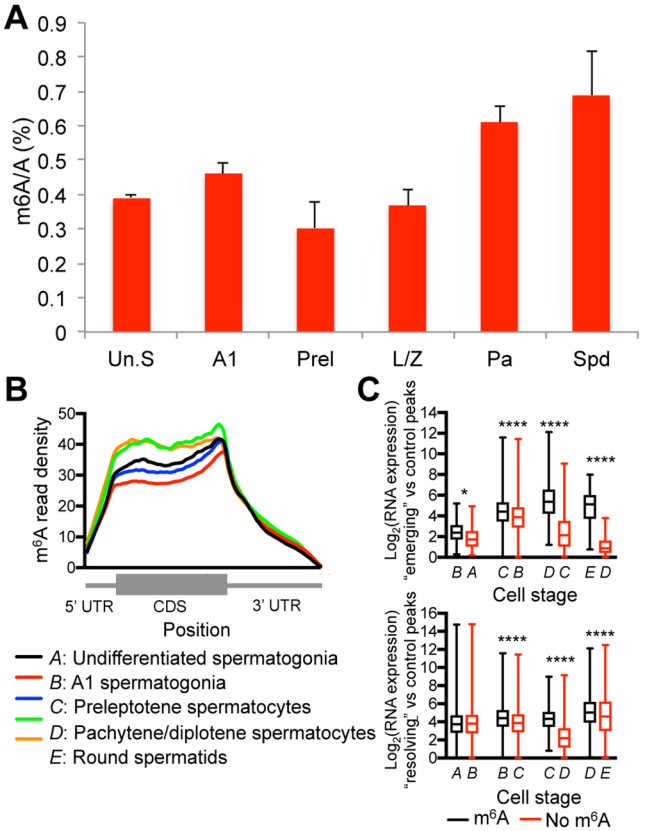

Figure 4 Dynamic change of m^{6}A during spermatogenesis. **(A)** m^{6}A LC–MS/MS quantification in six different developmental stages of spermatogonial cell. Un.S, undifferentiated spermatogonia; A1, type A1 spermatogonia; Prel, preleptotene spermatocytes; L/Z, lepotene/zygotene spermatocytes; Pa, Pachyotene/diplotene spermatocytes; Spd, round spermatids. The data show the mean ± SD of two biological replicates, $^{**}P < 0.01$, Student's *t*-test. **(B)** Metagene distribution of m^{6}A read density measured by m^{6}A-seq depicting the subtranscript distribution pattern of m^{6}A sites within the transcriptome of five different stages of spermatogenic cells. **(C)** RNA expression of transcripts with "emerging" or "resolving" peaks compared to unmethylated transcripts in five different stages of spermatogenic cells. A, undifferentiated spermatogonia; B, type A1 spermatogonia; C, preleptotene spermatocytes; D, pachytene/diplotene spermatocytes; E, round spermatids. "Emerging" peaks, m^{6}A peaks with greater enrichment (enrichment ratio > 2) upon differentiation from a previous stage; "Resolving" peaks, m^{6}A peaks with less enrichment (enrichment ratio < 0.5) upon differentiation to the next stage.

Next, we asked whether the presence of m^{6}A on a transcript affects its expression level. We identified "emerging" peaks that harbor greater enrichment in m^{6}A upon differentiation from a previous stage, as well as "resolving" peaks depleted in m^{6}A upon differentiation to the next stage. In both cases, methylated genes demonstrated greater expression compared to unmethylated genes; transcripts had greater expression levels when they developed "emerging" peaks, as well as when they contained "resolving" peaks (Figure 4C and Supplementary information, Figure S9C). Taken together, our results reveal that m^{6}A RNA modification is conserved and dynamically regulated during male germ cell development, suggesting its critical roles in spermatogenesis.

Knockout of either Mettl3 or Mettl14 results in dysregulation of translation in SSCs

Gene ontology (GO) analyses of m^{6}A methylome revealed that genes with their transcripts methylated fall into diverse functional groups (Supplementary information, Table S2). Notably, genes identified in each type of spermatogenic cells are highly enriched for their specific functions (Supplementary information, Table S3). We found that the majority of transcripts of genes that are reported to be required for SSC/progenitor cell proliferation and differentiation were methylated in the undifferentiated spermatogonia and type A_1 spermatogonia, including *Dnmt3b* [36], *Foxo1* [37], *Id4* [38], *Kit* [39], *Rptor* [40], *Sohlh2* [41], *Sox3* [42, 43], *Stat3* [44], *Stra8* [45, 46], and *Zbtb16* (*Plzf*) [47, 48] (Supplementary information, Table S3). Combined with SSC depletion in *Mettl3* or *Mettl14* single mutants, these data suggest that mRNA m^{6}A modification could control SSC development.

To gain more comprehensive insight into the mechanisms underlying SSC depletion, we conducted high-throughput RNA sequencing (RNA-seq) and ribosome profiling assays to analyze the transcriptome and translatome of THY1$^+$ undifferentiated spermatogonia from 5-day-old control, *Mettl3*-vKO, and *Mettl14*-vKO mutant testes, before overt morphological defects. The mutants had mild effects on transcript level (Supplementary information, Figure S10A). However, we identified 2 991 (1 416 up and 1 575 down) and 2 716 (1 258 up and 1 458 down) genes that were subjected to dysregulations of the TE (normalized read count of ribosome-protected fragments (RPFs)/mRNA fragments; Fold change > 2) upon either *Mettl3* or *Mettl14* deficiency, respectively, whereas the mRNA levels of most of these genes remained relatively stable (Figure 5A and 5B, Supplementary information, Table S4). Notably, these translationally dysregulated genes were exclusively enriched in those with transcripts bearing at least one m^{6}A peak (Figure 5C; Supplementary information, Table S4). Interestingly, *Mettl3*-vKO and *Mettl14*-vKO mutant SSCs/progenitor cells shared significant overlaps of the translationally up- or down-regulated genes (Figure 5D; Supplementary information, Figure S10B and Table S4),

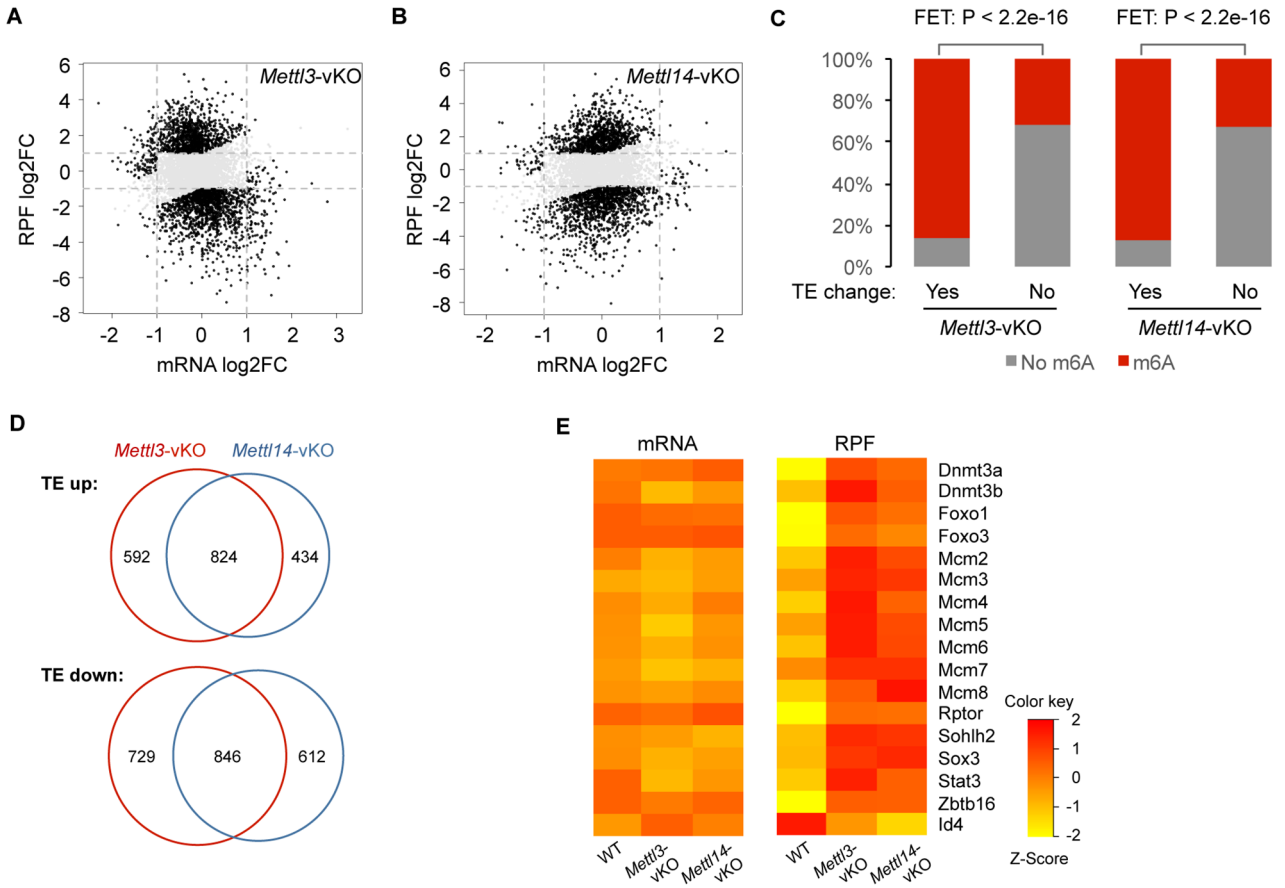

Figure 5 The mRNA translation dysregulations in the THY1$^+$ SSC/progenitor cells from the *Mettl3* and *Mettl14* single-mutants. **(A**, **B)** Scatter plots showing the fold changes of the RPF and mRNA of the genes in the THY1$^+$ SSC/progenitor cells upon *Mettl3* **(A)** or *Mettl14* **(B)** knockout. **(C)** Different proportions of the transcripts with m^{6}A modification in the genes with or without differential TE in the THY1$^+$ SSC/progenitor cells upon *Mettl3* (left) or *Mettl14* (right) knockout. The *P*-value of such difference was calculated with the Fisher's exact test. **(D)** Overlaps between the genes that are translationally up- (top) or down- (bottom) regulated upon *Mettl3* and *Mettl14* knockout. $P < 0.05$. **(E)** Heat maps showing the relative levels of the mRNA and RPF read counts of the selected genes, which are known to be involved in spermatogenesis, in the THY1$^+$ SSC/progenitor cells from the WT, *Mettl3*-vKO, and *Mettl14*-vKO mice.

further demonstrating that the two methyltransferases are functionally similar in SSCs/progenitor cells. Nevertheless, we cannot completely exclude the possibility that *Mettl3* may directly promote TE through interaction with the translation initiation machinery as shown in a recent study [17].

Importantly, the above methylated transcripts whose TE is significantly affected in mutant compared to control SSCs/progenitor cells include multiple genes essential for proliferation and differentiation (Figure 5E; Supplementary information, Figure S10C and S10D, Table S3). Among these genes, *Sohlh2* is known to control SSC/progenitor cell differentiation through repressing expression of genes implicated in SSC maintenance and inducing expression of genes involved in differentiation (Supplementary information, Figure S10D) [41]. Forced expression of *Dnmt3b* in the undifferentiated spermatogonia causes SSCs/progenitor cells to exit the undifferentiated status toward differentiation [36]. Consistent with hyperproliferation of SSCs in both mutants, TE for DNA replication factors such as MCM family proteins was significantly increased in mutants. Conversely, TE for *Id4*, which is required for SSCs [38], was significantly decreased in both mutants (Supplementary information, Figure S10D). Taken together, translational dysregulation of SSC/progenitor cell proliferation and differentiation regulators caused by disruption of the methyltransferase complex could lead to SSC phenotypes observed in *Mettl3* or *Mettl14* single mutants.

m^6A methyltransferases regulate TE of methylated mRNAs for spermiogenesis

To determine the roles of m^6A in spermatocytes and spermatids, we first performed GO analysis on genes containing "emerging" and "resolving" m^6A peaks in pachytene/diplotene spermatocytes and found that these genes are important for spermiogenesis, including cilium morphogenesis, cell projection organization, and CatSper complex formation, indicating that the methylated mRNAs transcribed in spermatocytes may be stored until they are required in elongating spermatid (Supplementary information, Table S5). Notably, most mRNAs that encode proteins previously reported to be essential for spermiogenesis were highly methylated in round spermatids and pachytene spermatocytes, respectively (Supplementary information, Table S3).

We next isolated pachytene spermatocytes and round spermatids from controls and *Mettls*-sKO mutants, and performed RNA-seq and ribosome profiling for transcriptome and translatome analysis. In line with the observed mild changes in mRNA levels of either *Mettl3* or *Mettl14* mutant SSCs/progenitor cells, combined deletion of both enzymes resulted in slight effects on mRNA levels in spermatocytes (n = 357 differentially expressed genes; P-value < 0.05) and round spermatids (n = 265 differentially expressed genes; P-value < 0.05) as compared to controls (Supplementary information, Figure S11A and S11B).

We then compared the gene TE between control and *Mettls*-sKO mutant spermatocytes, and round spermatids. We identified that 1 051 genes (556 up and 495 down) exhibited significant TE changes (P-value < 0.05 and TE change > 50%) in mutant spermatids compared to controls, while 1 287 genes (706 up and 581 down) showed significant TE changes in mutant spermatocytes (Figure 6A, Supplementary information, Figure S11C, Tables S6 and S7). Compared with genes that showed no change in TE, genes whose TE was significantly affected upon combined deletion of *Mettl3* and *Mettl14* showed significant enrichment of transcript methylation (Figure 6B, Supplementary information, Figure S11D, Tables S6 and S7).

Notably, in mutant spermatids, many genes with down-regulated TE are previously reported to be essential for spermiogenesis, including *Brd7* [49], *Cstf2t* [50], *Jmjd1c* [51], *Parp11* [52], *Lmtk2* [53], and *Tdrd12* [54] (Figure 6C). Among these genes, *Cstf2t* knockout (KO) resulted in defects resembling those found in OAT, as well as in *Mettls*-sKO mutants (Supplementary information, Figure S11E) [50]. Thus, translational inhibition of the key methylated transcripts of genes for spermiogenesis upon combined deletion of *Mettl3* and *Mettl14* may result in the observed OAT phenotypes in *Mettls*-sKO mutants. Interestingly, in mutant spermatocytes, genes with TE up-regulated include many factors for DNA replication and repair, which are required for early stage of spermatocytes but unnecessary for pachytenes (Supplementary information, Table S7), suggesting that m^6A may repress translation of overexpressed transcripts to prevent protein overproduction. Accordingly, in male germ cells, overexpression of *Gfer*, one of the genes with TE up-regulated, has been reported to cause male infertility [55]. Taken together, these results support the idea that m^6A modification could serve as a mark to promote translation for producing proteins essential for spermiogenesis, and inhibit translation for preventing deleterious consequences of overproducing proteins during late spermatogenesis.

Consistent with this hypothesis, we found that, according to the effect of m^6A on translation, the methylated transcripts could be divided into translation stimulated and repressed groups in mutant spermatids and spermatocytes. For example, in mutant spermatids, methylated transcripts with TE down-regulated are enriched for microtubule-based process, whereas genes with up-regulated TE are overpresented in metabolism and chromatin modification (Supplementary information, Figure S12A and S12B). In mutant spermatocytes, methylated transcripts with TE down-regulated are enriched for cilium formation, whereas the ones with TE up-regulated feature DNA metabolism and chromatin organization (Supplementary information, Figure S13A and S13B).

Discussion

Despite the recent extensive interest, dynamic regulation and functional roles of m^6A in mammals, particularly in mammalian development, remain largely uncharacterized. Here we present a comprehensive m^6A methylome landscape of developing male germ cells, as well as a detailed *in vivo* characterization of m^6A biogenesis and functions during mammalian spermatogenesis, providing new insights into spermatogenesis.

Our analyses of the m^6A methylome of spermatogenic cells at different developmental stages uncover transcripts that harbor extensive cell developmental stage-dependent common or unique m^6A RNA modification, and reveal the dynamic regulation of m^6A sites and the positive correlation of methylation with developmental stage-specific transcripts during spermatogenesis. These results will provide clues for further functional studies of m^6A RNA modification in germline development.

Our results reveal an essential role of m^6A RNA modification in the maintenance of SSC homeostasis. Early

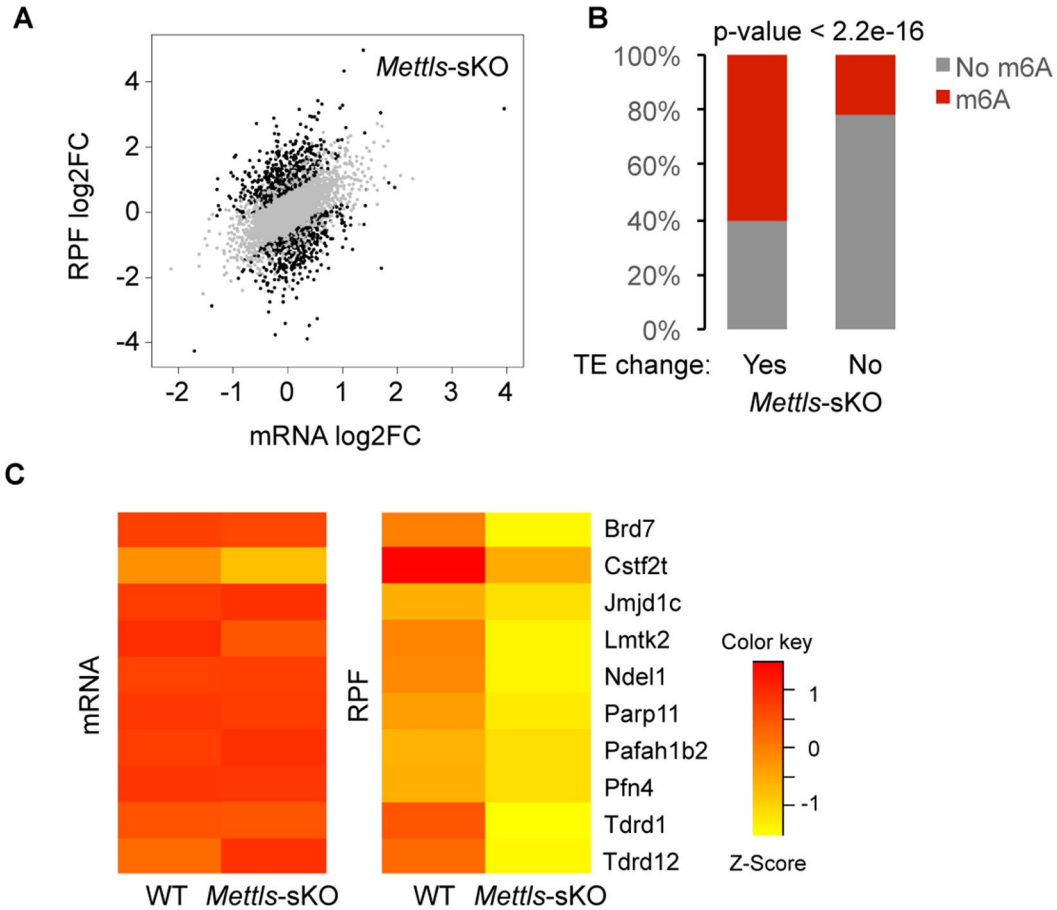

Figure 6 The mRNA translation dysregulations in spermatids from the *Mettl3* and *Mettl14* double mutants. **(A)** Scatter plot showing the fold changes of the RPF and mRNA of the genes in spermatids from the *Mettl3* and *Mettl14* double-mutant mice. **(B)** Different proportions of the transcripts with m^{6}A modification in the genes with or without differential TE in spermatids upon *Mettl3* and *Mettl14* double mutation. The *P*-value of such difference was calculated with the Fisher's exact test. **(C)** Heat maps showing the relative levels of the mRNA and RPF read counts of the selected genes, which are known to be involved in spermatogenesis (spermatids from the WT and *Mettls*-sKO mice).

germ cell-specific inactivation of either of the methyltransferases leads to loss of m^{6}A and impairs SSC/progenitor cell quiescence, resulting in rapid exhaustion of the SSC pool and complete germ cell-loss phenotype. m^{6}A profiling indicated that most key regulators of SSC/progenitor cells harbor extensive m^{6}A RNA modification, including *Plzf*, *Id4*, *Dnmt3b,* and *Sohlh2*. Despite subtle changes in mRNA levels, loss of m^{6}A upon either *Mettl3* or *Mettl14* deficiency caused translational dysregulation of those key regulators in SSC/progenitor cells. We propose that *Mettl3* or *Mettl14* maintain SSC/progenitor cell homeostasis through methylating transcripts of key regulators governing SSC proliferation and differentiation.

During the late stages of spermiogenesis, the transcripts inherited from spermatocytes and round spermatids could govern synthesis of proteins required for sperm development. Our analyses show heavy enrichment of m^{6}A in spermatids and spermatocytes, as well as substantial enrichment of the methylated transcripts in genes essential for spermiogenesis, revealing that m^{6}A-dependent RNA translation may act as a mechanism to control late stages of spermiogenesis. Consistent with this, conditional KO of both *Mettl3* and *Mettl14* caused translational downregulation of the key m^{6}A-modified transcripts for spermiogenesis, resulting in the defects in late stages of spermiogenesis. Thus, our work supports the idea that m^{6}A RNA modification could provide a mark to those transcripts, which in turn modulates their translation and storage during spermiogenesis.

Mice with conditional deletion of either *Mettl3* or *Mettl14* exhibit complete loss of SSCs, but show normal meiosis and spermatogenesis, indicating these enzymes

could have different or partially overlapping functions in late stages of spermatogenesis. Yeast *METTL3* orthologue *ime4* were shown to be essential for meiosis [28, 32-34]. In contrast to these studies, our results argue against an indispensable role for *Mettl3* and *Mettl14* in mouse meiosis because ablation of both genes in advanced germ cells only disrupts spermiogenesis without affecting meiosis. However, substantial enrichment of m^6A within meiosis-associated transcripts and dynamic changes of the methylated sites on these transcripts in different developmental stages of meiotic cells support the idea that m^6A RNA modification could regulate mouse meiosis, raising the question of whether more methyltransferases in addition to *Mettl3* and *Mettl14* contribute to the m^6A deposition on transcripts during mammalian meiosis. Accordingly, combined KO of both *Mettl3* and *Mettl14* did not significantly reduce m^6A levels in spermatocytes compared to single mutants. Thus, it is reasonable to speculate that diverse methyltransferases are present in cells in order to offer multiple ways to decorate transcripts with m^6A responsible for key biological functions. It would be interesting to further investigate whether a similar mechanism operates in other systems.

Collectively, our data indicate mRNA m^6A modification as a critical regulator to control the timely translation of groups of transcripts to coordinate proper production of proteins, which is essential for mammalian spermatogenesis. In the absence of either methyltransferase in early male germ cells, loss of m^6A leads to dysregulated translation of SSC/progenitor cell proliferation and differentiation factors, causing SSC depletion. Furthermore, *Mettl3*/*Mettl14* double mutants, but not single mutants, showed disrupted spermatid differentiation due to dysregulated translation of key factors for spermiogenesis, despite normal meiosis, which may suggest potential functional redundancy of these methyltransferase components in the late stages of the spermatogenesis program. Moreover, in addition to a role of m^6A in mRNA stability, our analyses indicate that m^6A on mRNA could provide an identity to transcripts for their coordinated translation, thus directing the proper expression of stage-specific genes during late spermatogenesis. We postulate that the precise effect of m^6A on translation might depend on its recognition by different reading mechanisms. It will be of interest to explore this hypothesis in the future.

Materials and Methods

Mice

The conditional mutant alleles for *Mettl3* and *Mettl14*, and the *Stra8-GFPCre* knockin mouse line were generated by the CRISPR/Cas9 technology. To generate a *Mettl3*-floxed line, in which exon 4 of the *Mettl3* allele is flanked by *loxP* sites, two independent guide RNAs targeting *Mettl3* introns 3 and 4 were designed. The donor vector containing exon 4 flanked by two *loxP* sites and two homology arms was used as a template. Two founder mice containing floxed exon 4 of *Mettl3* on the same allele were obtained. Using similar procedure, we obtained two founder mice containing floxed exon 2 of *Mettl14* on the same allele. Resulting founder male mice were mated to WT C57BL/6J (B6) female mice to obtain heterozygous *Mettl3*-floxed and *Mettl14*-floxed mice, respectively. Progeny were screened by PCR for germ line transmission of the targeted alleles. For conditional deletion of *Mettl3* or *Mettl14* in advanced germ cells, we established a *Stra8-GFPCre* knockin mouse line. A cDNA encoding the GFPCre fusion protein was inserted into the last coding exon of *Stra8*, and a 2A peptide sequence was included to link *Stra8* and *GFPCre* to allow expression of both genes. The *Stra8-GFPCre* lines were generated by Shanghai Biomodel Organism Co., Ltd. All mice described above were maintained on the C57BL/6J (B6) background. *Mettl3*- and *Mettl14*-floxed mice ($Mettl3^{flox/flox}$ and $Mettl14^{flox/flox}$) were then bred with germ cell-specific expressed Cre mice including *Vasa-Cre* mouse line (Jackson Laboratory, Bar Harbor, Maine, USA) and *Stra8-GFPCre* mouse line for excising the *loxP*-flanked exon 4 and exon 2 to generate germ cell-specific *Mettl3* and *Mettl14* KO mice, respectively. Germ cell-specific *Mettl3* and *Mettl14* double KO mice were obtained by crossing $Mettl3^{flox/flox}Mettl14^{flox/flox}$ with $Mettl3^{flox/+}Mettl14^{flox/+}$ or $Mettl3^{flox/+}Mettl14^{flox/flox}$ carried germ cell-specific expressed Cre mice. All of the primers for PCR genotyping were listed in Supplementary information, Table S8. All animal experiments were conducted in accordance with the guidelines in the Animal Care and Use Committee at Shanghai Institute of Biochemistry and Cell Biology, Chinese Academy of Science.

Isolation of spermatogenic cells

We used male mice in B6 background for preparations of different types of spermatogenic cells from undifferentiated spermatogonia, type A_1 spermatogonia, preleptotene spermatocyte, pachytene/diplotene spermatocyte, and round spermatid. Isolation of the undifferentiated spermatogonia, $THY1^+$ spermatogonia, from 5-7-day-old mice was carried out using magnetic-activated cell sorting (MACS) as described previously [56]. *Stra8-GFPCre* mice were used for synchronous spermatogenesis to generate type A_1 spermatogonia and preleptotene spermatocytes, respectively. Spermatogenesis was synchronized as previously described with modifications [57]. Briefly, 2-dpp *Stra8-GFPCre* mice were pipette fed with 100 μg/g body weight WIN 18 446 (Sigma), suspended in 1% gum tragacanth, for 7 consecutive days. At Day 8 of WIN 18 446 treatments, these animals received an i.p. injection of RA (Sigma; 30 μg/g body weight) in dimethyl sulfoxide (DMSO), and were then left to recover for 24 h. Type A_1 spermatogonia were then collected based on their GFP fluorescence label using fluorescence-activated cell sorting (FACS) (Becton Dickinson). Spermatocytes and round spermatid from adult mice were collected based on Ho33342/PI staining using FACS as previously described [58].

Histological and immunohistochemical analyses

Testes were fixed in Bouin's buffer or 4% paraformaldehyde (PFA), embedded in paraffin and sectioned. Sections were deparaffinized, rehydrated, and stained with hematoxylin and eosin

(H&E). For immunofluorescence analysis, sections were boiled in 10 mM sodium citrate buffer (pH 6.0) for 15 min, brought to room temperature, washed in PBS with 0.1% Triton X-100. The sections were then blocked with blocking buffer (10% donkey serum and 0.1% Triton X-100 in PBS) for 60 min at room temperature, and later incubated with the primary antibodies in blocking buffer overnight at 4 °C. The following primary antibodies were used in this study: rabbit anti-METTL3(1:200; Abcam), rabbit anti-METTL14(1:200; Sigma), rabbit anti-PLZF (1:100; Santa Cruz Biotechnology), goat anti-LIN28a (1:200; R&D Systems), goat anti-GFRα1 (1:50; R&D Systems), rabbit anti-SOX9 (1:200; Millipore), rabbit anti-STRA8 (1:200; gift from Michael Griswold, Washington State University, Pullman, WA), mouse anti-γH2AX (1:200; Millipore), rat anti-GCNA IgM (1:50; kindly provided by Dr G Enders, University of Kansas, Kansas City, KS), rabbit anti-VASA (1:100; Abcam), rabbit anti-DMC1 (1:100; Santa Cruz Biotechnology), and FITC-conjugated peanut agglutinin (1:500; Sigma). On the following day, slides were washed four times for 15 min in PBS with 0.1% Triton X-100, and Alexa Fluor 488- and Alexa Fluor 594-conjugated donkey secondary antibody (Jackson ImmunoResearch Laboratories) were then added at a 1:500 dilution. After 60 min at room temperature, the sections were washed in PBS, rinsed quickly in pure ethanol, mounted in Prolong Gold Antifade medium with DAPI (Molecular Probes), and then analyzed by fluorescence microscopy (Olympus) or confocal microscopy (Olympus). Apoptotic cells were detected using an In Situ Cell Death Detection Kit, Fluorescein (Roche Applied Science) according to the manufacturer's instructions.

Whole-mount immunohistochemistry

Mouse testes were removed from the tunica albuginea, and untangled seminiferous tubules were fixed in 4% PFA with 0.5 mM $CaCl_2$, and PBS on ice for 4 h. The seminiferous tubules were washed in PBS with 0.2% NP40 (Sigma) for 20 min, and dehydrated through a graded methanol series (25, 50, 75, and 100%) in PBS containing 0.1% Tween 20 (Sigma) (PBST) on ice for 1 h each. After rehydration in PBST for 5 min twice, the tubules were blocked in blocking buffer (1% bovine serum albumin (BSA) and 4% donkey serum in PBST) for 1 h, and incubated with primary antibodies against GFRA1 (1:50), LIN28A (1:200), and PLZF (1:100) in blocking buffer at 4 °C overnight. After washed in PBST, the tubules were incubated with Alexa Fluor 488- and Alexa Fluor 594-conjugated donkey secondary antibody (Jackson ImmunoResearch) for 2 h at room temperature. The tubules were then washed in PBST, mounted, and observed using confocal microscopy (Olympus).

For EdU labeling, as described previously, mice were i.p. injected with EdU (Invitrogen) (50 μg/g body weight) in PBS [59]. The mice were killed 2 h later and testes were removed and treated either for sections or whole-mount staining. The samples were immunostained with primary antibody first, and then detected for the EdU incorporation by Click-It EdU Alexa Fluor 594 Imaging Kit according to the manufacturer's protocol (Invitrogen).

CASA

Cauda epididymides from control and *Mettl*-sKO double mutants were minced at 37 °C in 1 ml of Dulbecco Modified Eagle Medium (Invitrogen) supplemented with 3% BSA. After 5 min at 37 °C, tissue was removed, and aliquots of sperm suspension were diluted with fresh medium to adjust an approximate concentration to 6 million/ml, and CASA was performed using the HTM-IVOS system (Version 10.8; Hamilton-Thorne Research). At least 1 000 spermatozoa and 10 fields were assessed for each specimen (n = 5-6 independent experiments), and the percentages of motile and progressively motile spermatozoa were determined.

RNA isolation

Total RNA isolation for UPLC-MS/MS analysis: total RNA was isolated with Trizol reagent (Invitrogen). mRNA was extracted using GenElute mRNA miniprep (Sigma-Aldrich) followed by further removal of contaminated rRNA by using RiboMinus Transcriptome Isolation Kit (Invitrogen) according to the manufacturer's instructions. mRNA concentration was measured by Qubit.

mRNA-seq

Total RNA was isolated from THY1$^+$KIT$^-$ spermatogonia, spermatocytes, and spermatids from control and germ-cell mutant mice using Trizol reagent (Invitrogen). RNA purification and libraries of cDNA were constructed by the Omics Core of CAS-MPG Partner Institute for Computational Biology at Shanghai Institutes for Biological Sciences using the TrueSeq Stranded Total RNA Library Prep Kit (Illumina) following manufacturer's instructions. Libraries were sequenced using single reads (100 nt) on an Illumina HiSeq 2000. Sequencing reads were mapped to the ENSEMBL Mouse Reference Genome (GRCm38 release 87) using STAR (version 2.5.1) with the following parameters: --alignEndsType EndToEnd--outFilterMismatchNmax1--outFilterMultimapNmax 5--outSAMtype BAM SortedByCoordinate. Read assignment and counting were achieved using HTSeq-count (version 0.7.2) in intersection-strict mode [60].

UPLC-MS/MS analysis of m^{6}A levels

About 50-100 ng of purified mRNA was digested by nuclease P1 (1U; Sigma) in 20 μl of buffer containing 10 mM of NH_4Ac (pH 5.3) at 42 ºC for 4 h. About 100 mM NH_4HCO_3 and alkaline phosphatase (0.5 U) were then added to the reaction for another incubation at 37 °C for 4 h. The digested sample was centrifuged at 4 °C, 13 000 rpm for 20 min and the supernatant was injected into UPLC-MS/MS. The nucleosides were separated by UPLC (SHIMADZU) equipped with ZORBAX SB-Aq column (Agilent), and detected with Triple Quad 5500 (AB SCIEX) in positive ion multiple reaction-monitoring (MRM) mode. Quantitation of modifications was based on nucleoside-to-base ion mass transitions: *m/z* 268.0-136.0 for A, and *m/z* 282.0-150.1 for m^{6}A. Pure nucleosides were used to generate standard curves, from which the concentrations of A and m^{6}A in the sample were calculated. The level of m^{6}A was then calculated as a percentage of total unmodified A.

m^{6}A-seq

m^{6}A-seq was performed as previously described [6]. Briefly, spermatogonial cells were isolated as described above. PolyA mRNA was enriched using GenElute mRNA Miniprep Kit following the manufacturer's protocols. mRNA was sonicated to ~100 nt, mixed with 2.5 mg affinity-purified anti-m^{6}A polyclonal antibody (Synaptic Systems) in IP buffer (150 mM NaCl, 0.1% NP-40, and 10 mM Tris-HCl, pH 7.4), and incubated for 2 h at 4 °C. The antibody-RNA complex was isolated by incubation with protein A beads (Invitrogen) at 4 °C for 2 h. The beads were washed three

times and eluted competitively with an m^6A monophosphate solution. RNA in the eluate was isolated using RNA Clean and Concentrator (Zymo Research) and used for library preparation with TruSeq stranded mRNA sample preparation kit (Illumina).

Data analyses were performed as previously described [8, 14]. Briefly, after removing adapters, sequencing reads were aligned to the reference genome (mm10) using TopHat (v2.0.14) [61]. The longest isoform was used if multiple isoforms were detected. Aligned reads were extended to 100 nt (average fragment size) and converted from genome-based coordinates to isoform-based coordinates to eliminate interference from introns in peak calling. To call m^6A peaks, the longest isoform of each human gene was scanned using a 100 nt sliding window with 10 nt steps. To reduce bias from potentially inaccurate gene structure annotation and the arbitrary usage of the longest isoform, windows with read counts < 1/20 of the top window in both m^6A IP and input sample were excluded. For each gene, the read count in each window was normalized by the median count of all windows of that gene. A negative binomial model was used to identify the differential windows between IP and input samples by using the edgeR [62]. The window was called positive if FDR < 1% and log2 (enrichment score) ≥ 1. Overlapping positive windows were merged. The following four numbers were calculated to obtain the enrichment score of each peak (or window): (a) read count of the IP sample in the current peak/window, (b) median read count of the IP sample in all 100 nt windows on the current mRNA, (c) read count of the input sample in the current peak/window, and (d) median read count of the input sample in all 100 nt windows on the current mRNA. The enrichment score of each window was calculated as (a × d)/(b × c). When comparing the m^6A profiles between different samples to determine "emerging" and "resolving" peaks, a peak (m^6A IP/input > 2) was considered "enriched" if its enrichment ratio was > 2.

Ribosome profiling and total RNA sequencing in parallel

Cells were washed with prechilled PBS (with 100 μg/ml cycloheximide, Sigma-Aldrich) and then harvested by centrifugation at 4 °C (2 000 rpm, 5 min). Cell pellet of each sample was resolved in prechilled lysis buffer (20 mM Tris-HCl (pH 7.4), 150 mM NaCl, 5 mM $MgCl_2$, 0.1% NP-40, 1% Triton X-100, 1 mM DTT, 25 U/ml of RNase-free DNAse I, and 100 μg/ml cycloheximide). After 10 min of incubation on ice with periodic agitation, the lysate was centrifuged for 10 min (20 000× *g* at 4 °C), and the supernatant was collected.

The libraries for paralleled ribosome profiling and total RNA-seq were prepared as previously described [63, 64]. Briefly, the total RNA was isolated from 50 μl of the cell lysate using the Acid Phenol: chloroform extraction method and heat fragmented at 95 °C for 25 min. The ribosome protected RNA fragments (RPF) were obtained from 100 μl of the cell lysate treated with 60 U/A260 of RNase I, and further purified with Sephacryl S400 columns (GE Healthcare). Finally, the RPFs with the length of 25-35 nt were selected on a 15% Urea-Polyacrylamide gel. Next, the same procedure was followed to prepare the sequencing libraries from both the total RNA fragments and the RPFs. This includes 3′ adaptor ligation, reverse transcription, circularization of the cDNA, and PCR amplification [63, 64]. The libraries were then sequenced on the Illumina HiSeq 2 500 system with 50 cycles of single-end reading.

Ribosome profiling data analysis

The pre-processing procedure of the ribosome profiling and the paralleled RNA-seq data has been described previously [65]. Specifically, the cutadapt program [66] was used to trim the 3′ adaptor in the raw reads of both mRNA and RPF. Low-quality reads with Phred quality scores lower than 25 (> 75% of bases) were removed using the fastx quality filter (http://hannonlab.cshl.edu/fastx_toolkit/). Next, sequencing reads originating from rRNAs were identified and discarded by aligning the reads to rRNA sequences of the particular species using Bowtie (version 1.1.2) with no mismatch allowed. The remaining reads were then mapped to the mouse genome (GRCm38 (Ensembl release 87)) and spliced transcripts using STAR (version 2.5.1) with the following parameters: --alignEndsType EndToEnd --outFilterMismatchNmax 1 --outFilterMultimapNmax 5 --outSAMtype BAM SortedByCoordinate. To control the noise from multiple alignments, reads mapped to multiple genomic positions were discarded.

For each gene, mRNA expression was estimated by the RNA-seq reads, which were counted using HTSeq-count (version 0.7.2) [60] in intersection-strict mode. For quantification of RPF, multiple filters were implemented on raw reads to reduce the technical noise of ribosome profiling and extract the reads originating from ribosome-binding and translating sequences in coding regions. First, RPF reads with length between 25 and 35 nt were deemed high quality and most likely to be from ribosome occupation in mammalian cells [67, 68]. Second, to reduce noise due to multiple alignments, only the reads uniquely mapped to the coding regions were counted as RPFs. Third, due to the potential accumulation of ribosomes around the starts and ends of coding regions [68, 69], reads aligned to the first 15 and last 5 codons were excluded for the counting of RPFs. Finally, The Xtail package [65] was used to identify the genes subjected to differential translation. For the various gene sets selected by the different analysis, GO enrichment analysis was conducted using the tool Metascape. The GO terms with *P*-values < 0.001 were selected and imported into REVIGO, which visualizes the terms as nodes in a network [70]. Each GO term was color-coded according to the *P*-value (–log10). The size of each node is proportional to the number of genes belong to the GO term, whereas the link between different terms represent the number of shared genes.

Acknowledgments

M-HT was supported by the Strategic Priority Research Program of the Chinese Academy of Sciences (XDB19000000), the Ministry of Science and Technology of China (2014CB943101), the National Key Research and Development Program of China (2016YFC1000600), SIBS foundation, the National Natural Science Foundation of China (31471401 and 31671553), the Science and Technology Commission of Shanghai Municipality (14140901502 and 14JC1407100). This work was also supported by NIH HG008688 (CH). CH is an investigator of the Howard Hughes Medical Institute. XY was supported by the National Natural Science Foundation of China (81472855 and 91540109), the Ministry of Science and Technology of China Grant (2016YFC0906001). We thank the Histology, Flow Cytometry and Vivarium services at SIBCB, and the Genome Sequencing and High-performance Computing services from the National Protein Science Facility (Beijing) at Tsinghua University.

Author Contributions

M-HT conceived the project, and with CH and XY, designed the project and data analysis. M-HT, CH, and XY wrote the manuscript with contributions from all authors. ZL conducted phenotype analysis, and isolated spermatogonial cells and RNAs for all experiments in the project. PJH and ZL conducted m^{6}A-seq and analysis. XX, JF, QZ, and WS conducted ribosome profiling experiments and data analysis. K-JZ, TZ, YZ assisted in cell isolation and phenotype analysis. XZ and GJ carried out m^{6}A-LS/MS analysis. YZ conducted CASA assay.

Competing Financial Interests

The authors declare no competing financial interests.

References

1 Griswold MD. Spermatogenesis: the commitment to meiosis. *Physiol Rev* 2016; **96**: 1-17.
2 Clermont Y. Kinetics of spermatogenesis in mammals: seminiferous epithelium cycle and spermatogonial renewal. *Physiol Rev* 1972; **52**: 198-236.
3 Oatley JM, Brinster RL. Regulation of spermatogonial stem cell self-renewal in mammals. *Annu Rev Cell Dev Biol* 2008; **24**: 263-286.
4 Kleene KC. Connecting *cis*-elements and *trans*-factors with mechanisms of developmental regulation of mRNA translation in meiotic and haploid mammalian spermatogenic cells. *Reproduction* 2013; **146**:R1-R19.
5 Alarcon CR, Goodarzi H, Lee H, Liu X, Tavazoie S, Tavazoie SF. HNRNPA2B1 is a mediator of m(6)A-dependent nuclear RNA processing events. *Cell* 2015; **162**:1299-1308.
6 Dominissini D, Moshitch-Moshkovitz S, Schwartz S, *et al.* Topology of the human and mouse m6A RNA methylomes revealed by m6A-seq. *Nature* 2012; **485**:201-206.
7 Meyer KD, Saletore Y, Zumbo P, Elemento O, Mason CE, Jaffrey SR. Comprehensive analysis of mRNA methylation reveals enrichment in 3′ UTRs and near stop codons. *Cell* 2012; **149**:1635-1646.
8 Wang X, Zhao BS, Roundtree IA, *et al.* N^6-methyladenosine modulates messenger RNA translation efficiency. *Cell* 2015; **161**:1388-1399.
9 Wei CM, Gershowitz A, Moss B. Methylated nucleotides block 5′ terminus of HeLa cell messenger RNA. *Cell* 1975; **4**:379-386.
10 Wang X, Lu Z, Gomez A, *et al.* N^6-methyladenosine-dependent regulation of messenger RNA stability. *Nature* 2014; **505**:117-120.
11 Zhou J, Wan J, Gao X, Zhang X, Jaffrey SR, Qian SB. Dynamic m^{6}A mRNA methylation directs translational control of heat shock response. *Nature* 2015; **526**:591-594.
12 Xiang Y, Laurent B, Hsu CH, *et al.* RNA m^{6}A methylation regulates the ultraviolet-induced DNA damage response. *Nature* 2017; **543**:573-576.
13 Fustin JM, Doi M, Yamaguchi Y, *et al.* RNA-methylation-dependent RNA processing controls the speed of the circadian clock. *Cell* 2013; **155**:793-806.
14 Zhao BS, Wang X, Beadell AV, *et al.* m^{6}A-dependent maternal mRNA clearance facilitates zebrafish maternal-to-zygotic transition. *Nature* 2017; **542**:475-478.
15 Zhang S, Zhao BS, Zhou A, *et al.* m^{6}A Demethylase ALKBH5 maintains tumorigenicity of glioblastoma stem-like cells by sustaining FOXM1 expression and cell proliferation program. *Cancer Cell* 2017; **31**:591-606 e596.
16 Cui Q, Shi H, Ye P, *et al.* m^{6}A RNA methylation regulates the self-renewal and tumorigenesis of glioblastoma stem cells. *Cell Rep* 2017; **18**:2622-2634.
17 Lin S, Choe J, Du P, Triboulet R, Gregory RI. The m^{6}A methyltransferase METTL3 promotes translation in human cancer cells. *Mol Cell* 2016; **62**:335-345.
18 Bokar JA, Shambaugh ME, Polayes D, Matera AG, Rottman FM. Purification and cDNA cloning of the AdoMet-binding subunit of the human mRNA (N^6-adenosine)-methyltransferase. *RNA* 1997; **3**:1233-1247.
19 Liu J, Yue Y, Han D, *et al.* A METTL3-METTL14 complex mediates mammalian nuclear RNA N^6-adenosine methylation. *Nat Chem Biol* 2014; **10**:93-95.
20 Ping XL, Sun BF, Wang L, *et al.* Mammalian WTAP is a regulatory subunit of the RNA N^6-methyladenosine methyltransferase. *Cell Res* 2014; **24**:177-189.
21 Jia G, Fu Y, Zhao X, *et al.* N^6-methyladenosine in nuclear RNA is a major substrate of the obesity-associated FTO. *Nat Chem Biol* 2011; **7**:885-887.
22 Zheng G, Dahl JA, Niu Y, *et al.* ALKBH5 is a mammalian RNA demethylase that impacts RNA metabolism and mouse fertility. *Mol Cell* 2013; **49**:18-29.
23 Geula S, Moshitch-Moshkovitz S, Dominissini D, *et al.* Stem cells. m^{6}A mRNA methylation facilitates resolution of naive pluripotency toward differentiation. *Science* 2015; **347**:1002-1006.
24 Wang Y, Li Y, Toth JI, Petroski MD, Zhang Z, Zhao JC. N^6-methyladenosine modification destabilizes developmental regulators in embryonic stem cells. *Nat Cell Biol* 2014; **16**:191-198.
25 Haussmann IU, Bodi Z, Sanchez-Moran E, *et al.* m^{6}A potentiates Sxl alternative pre-mRNA splicing for robust Drosophila sex determination. *Nature* 2016; **540**:301-304.
26 Lence T, Akhtar J, Bayer M, *et al.* m^{6}A modulates neuronal functions and sex determination in Drosophila. *Nature* 2016; **540**:242-247.
27 Hongay CF, Orr-Weaver TL. Drosophila inducer of MEiosis 4 (IME4) is required for Notch signaling during oogenesis. *Proc Natl Acad Sci USA* 2011; **108**:14855-14860.
28 Schwartz S, Agarwala SD, Mumbach MR, *et al.* High-resolution mapping reveals a conserved, widespread, dynamic mRNA methylation program in yeast meiosis. *Cell* 2013; **155**:1409-1421.
29 Gallardo T, Shirley L, John GB, Castrillon DH. Generation of a germ cell-specific mouse transgenic Cre line, *Vasa-Cre*. *Genesis* 2007; **45**:413-417.
30 Roundtree IA, Evans ME, Pan T, He C. Dynamic RNA modifications in gene expression regulation. *Cell* 2017; **169**:1187-1200.
31 Wang X, Feng J, Xue Y, *et al.* Structural basis of N^6-adenosine methylation by the METTL3-METTL14 complex. *Nature* 2016; **534**:575-578.
32 Clancy MJ, Shambaugh ME, Timpte CS, Bokar JA. Induction of sporulation in *Saccharomyces cerevisiae* leads to the formation of N^6-methyladenosine in mRNA: a potential mech-

anism for the activity of the IME4 gene. *Nucleic Acids Res* 2002; **30**:4509-4518.
33 Shah JC, Clancy MJ. IME4, a gene that mediates MAT and nutritional control of meiosis in *Saccharomyces cerevisiae*. *Mol Cell Biol* 1992; **12**:1078-1086.
34 Agarwala SD, Blitzblau HG, Hochwagen A, Fink GR. RNA methylation by the MIS complex regulates a cell fate decision in yeast. *PLoS Genet* 2012; **8**:e1002732.
35 Pendleton KE, Chen B, Liu K, *et al.* The U6 snRNA m^6A methyltransferase METTL16 regulates SAM synthetase intron retention. *Cell* 2017; **169**:824-835 e814.
36 Shirakawa T, Yaman-Deveci R, Tomizawa S, *et al.* An epigenetic switch is crucial for spermatogonia to exit the undifferentiated state toward a Kit-positive identity. *Development* 2013; **140**:3565-3576.
37 Goertz MJ, Wu Z, Gallardo TD, Hamra FK, Castrillon DH. Foxo1 is required in mouse spermatogonial stem cells for their maintenance and the initiation of spermatogenesis. *J Clin Invest* 2011; **121**:3456-3466.
38 Chan F, Oatley MJ, Kaucher AV, *et al.* Functional and molecular features of the Id4+ germline stem cell population in mouse testes. *Genes Dev* 2014; **28**:1351-1362.
39 Schrans-Stassen BH, van de Kant HJ, de Rooij DG, van Pelt AM. Differential expression of c-kit in mouse undifferentiated and differentiating type A spermatogonia. *Endocrinology* 1999; **140**:5894-5900.
40 Wang M, Guo Y, Wang M, *et al.* The glial cell-derived neurotrophic factor (GDNF)-responsive phosphoprotein landscape identifies raptor phosphorylation required for spermatogonial progenitor cell proliferation. *Mol Cell Proteomics* 2017; **16**:982-997.
41 Hao J, Yamamoto M, Richardson TE, *et al.* Sohlh2 knockout mice are male-sterile because of degeneration of differentiating type A spermatogonia. *Stem Cells* 2008; **26**:1587-1597.
42 Laronda MM, Jameson JL. Sox3 functions in a cell-autonomous manner to regulate spermatogonial differentiation in mice. *Endocrinology* 2011; **152**:1606-1615.
43 Weiss J, Meeks JJ, Hurley L, Raverot G, Frassetto A, Jameson JL. Sox3 is required for gonadal function, but not sex determination, in males and females. *Mol Cell Biol* 2003; **23**:8084-8091.
44 Oatley JM, Kaucher AV, Avarbock MR, Brinster RL. Regulation of mouse spermatogonial stem cell differentiation by STAT3 signaling. *Biol Reprod* 2010; **83**:427-433.
45 Zhou Q, Li Y, Nie R, *et al.* Expression of stimulated by retinoic acid gene 8 (Stra8) and maturation of murine gonocytes and spermatogonia induced by retinoic acid *in vitro*. *Biol Reprod* 2008; **78**:537-545.
46 Zhou Q, Nie R, Li Y, *et al.* Expression of stimulated by retinoic acid gene 8 (Stra8) in spermatogenic cells induced by retinoic acid: an *in vivo* study in vitamin A-sufficient postnatal murine testes. *Biol Reprod* 2008; **79**:35-42.
47 Buaas FW, Kirsh AL, Sharma M, *et al.* Plzf is required in adult male germ cells for stem cell self-renewal. *Nat Genet* 2004; **36**:647-652.
48 Costoya JA, Hobbs RM, Barna M, *et al.* Essential role of Plzf in maintenance of spermatogonial stem cells. *Nat Genet* 2004; **36**:653-659.
49 Wang H, Zhao R, Guo C, *et al.* Knockout of BRD7 results in impaired spermatogenesis and male infertility. *Sci Rep* 2016; **6**:21776.
50 Dass B, Tardif S, Park JY, *et al.* Loss of polyadenylation protein tauCstF-64 causes spermatogenic defects and male infertility. *Proc Natl Acad Sci USA* 2007; **104**:20374-20379.
51 Kuroki S, Akiyoshi M, Tokura M, *et al.* JMJD1C, a JmjC domain-containing protein, is required for long-term maintenance of male germ cells in mice. *Biol Reprod* 2013; **89**:93.
52 Meyer-Ficca ML, Ihara M, Bader JJ, Leu NA, Beneke S, Meyer RG. Spermatid head elongation with normal nuclear shaping requires ADP-ribosyltransferase PARP11 (ARTD11) in mice. *Biol Reprod* 2015; **92**:80.
53 Kawa S, Ito C, Toyama Y, *et al.* Azoospermia in mice with targeted disruption of the Brek/Lmtk2 (brain-enriched kinase/lemur tyrosine kinase 2) gene. *Proc Natl Acad Sci USA* 2006; **103**:19344-19349.
54 Pandey RR, Tokuzawa Y, Yang Z, *et al.* Tudor domain containing 12 (TDRD12) is essential for secondary PIWI interacting RNA biogenesis in mice. *Proc Natl Acad Sci USA* 2013; **110**:16492-16497.
55 Cao Y, Fu YL, Ge CH, *et al.* Mice overexpression of human augmenter of liver regeneration (hALR) in male germ cells shows abnormal spermatogenesis and reduced fertility. *Endocr J* 2012; **59**:989-999.
56 Tong MH, Mitchell DA, McGowan SD, Evanoff R, Griswold MD. Two miRNA clusters, Mir-17-92 (Mirc1) and Mir-106b-25 (Mirc3), are involved in the regulation of spermatogonial differentiation in mice. *Biol Reprod* 2012; **86**:72.
57 Hogarth CA, Evanoff R, Mitchell D, *et al.* Turning a spermatogenic wave into a tsunami: synchronizing murine spermatogenesis using WIN 18,446. *Biol Reprod* 2013; **88**:40.
58 Gaysinskaya V, Soh IY, van der Heijden GW, Bortvin A. Optimized flow cytometry isolation of murine spermatocytes. *Cytometry A* 2014; **85**:556-565.
59 Chen Y, Ma L, Hogarth C, Wei G, Griswold MD, Tong MH. Retinoid signaling controls spermatogonial differentiation by regulating expression of replication-dependent core histone genes. *Development* 2016; **143**:1502-1511.
60 Anders S, Pyl PT, Huber W. HTSeq--a Python framework to work with high-throughput sequencing data. *Bioinformatics* 2015; **31**:166-169.
61 Kim D, Pertea G, Trapnell C, Pimentel H, Kelley R, Salzberg SL. TopHat2: accurate alignment of transcriptomes in the presence of insertions, deletions and gene fusions. *Genome Biol* 2013; **14**:R36.
62 Robinson MD, McCarthy DJ, Smyth GK. edgeR: a Bioconductor package for differential expression analysis of digital gene expression data. *Bioinformatics* 2010; **26**:139-140.
63 Ingolia NT, Brar GA, Rouskin S, McGeachy AM, Weissman JS. The ribosome profiling strategy for monitoring translation *in vivo* by deep sequencing of ribosome-protected mRNA fragments. *Nat Protoc* 2012; **7**:1534-1550.
64 Ingolia NT, Ghaemmaghami S, Newman JR, Weissman JS. Genome-wide analysis *in vivo* of translation with nucleotide resolution using ribosome profiling. *Science* 2009; **324**:218-223.
65 Xiao Z, Zou Q, Liu Y, Yang X. Genome-wide assessment of differential translations with ribosome profiling data. *Nat Commun* 2016; **7**:11194.

66 Martin M. Cutadapt removes adapter sequences from high-throughput sequencing reads. *EMBnet J* 2011; **17**:10-12.
67 Crappe J, Ndah E, Koch A, *et al.* PROTEOFORMER: deep proteome coverage through ribosome profiling and MS integration. *Nucleic Acids Res* 2015; **43**:e29.
68 Ingolia NT, Brar GA, Stern-Ginossar N, *et al.* Ribosome profiling reveals pervasive translation outside of annotated protein-coding genes. *Cell Rep* 2014; **8**:1365-1379.
69 Ingolia NT, Lareau LF, Weissman JS. Ribosome profiling of mouse embryonic stem cells reveals the complexity and dynamics of mammalian proteomes. *Cell* 2011; **147**:789-802.
70 Supek F, Bosnjak M, Skunca N, Smuc T. REVIGO summarizes and visualizes long lists of gene ontology terms. *PLoS One* 2011; **6**:e21800.

(**Supplementary information** is linked to the online version of the paper on the *Cell Research* website.)